

Exciton Dynamics and Biexciton Formation in Single-Walled Carbon Nanotubes Studied with Femtosecond Transient Absorption Spectroscopy

David J. Styers-Barnett,[†] Stephen P. Ellison,[†] Brian P. Mehl,[†] Brittany C. Westlake,[†] Ralph L. House,[†] Cheol Park,[‡] Kristopher E. Wise,[‡] and John M. Papanikolas^{*,†}

Department of Chemistry, Venable and Kenan Laboratories, University of North Carolina at Chapel Hill, Chapel Hill, North Carolina 27599, and National Institute of Aerospace, NASA Langley Research Center, MS 226, Hampton, Virginia 23681

Received: October 11, 2007; In Final Form: December 12, 2007

We used femtosecond transient absorption (TA) spectroscopy to examine the excited state dynamics of single-walled carbon nanotube (SWNT) bundles embedded in polymer matrices. The SWNTs were excited by a femtosecond pump pulse centered at either 1800, 900, or 550 nm and probed using a white-light continuum extending from 400 to 750 nm. We observed a structured TA spectrum consisting of a series of narrow induced transmission (IT) and induced absorption (IA) bands. The TA spectrum, which is independent of excitation wavelength, appeared on a time scale shorter than our instrument response (200 fs) and persisted for up to 100 ps. TA spectra obtained at a series of pump–probe delay times provided a window through which to monitor the exciton dynamics. We observed three distinct spectral signatures in the time-dependent data: (1) the decay of a broad photobleach, (2) the biphasic decay of narrow IT and IA features, and (3) a dynamical spectral shift of IA bands. These processes were attributed to plasmon relaxation, electron–hole recombination, and lattice relaxation associated with exciton self-trapping, respectively. Analysis of the transient spectrum suggested that it arose from a nonlinear optical response of the SWNT, where excitons produced by the pump pulse modified the transition frequencies of subsequent carrier excitations. The result was a series of IT bands (bleaches) at the ground state absorption frequencies, and associated with each was a corresponding red-shifted absorption band. These induced absorptions were attributed to the formation of biexcitons, four-particle excitations that are produced through the sequential excitation of two closely spaced electron–hole pairs.

Introduction

Single-walled carbon nanotubes (SWNTs) possess unique chemical and physical properties^{1,2} that hold promise for developing new materials with enhanced mechanical, electronic, and optical capabilities. Because of their enormous strength and large electrical conductivity, SWNTs have been targeted for use in high-strength composites, nanometer-sized electronic devices, efficient photovoltaics, photoconductors, optoelectronic materials, and nanosensors.^{3–19} Furthermore, their large nonlinear susceptibilities and fast carrier relaxation times could make them a central component in ultrafast, all-optical switching devices used in optical communication networks.^{20–22} Motivated by their unique characteristics and promise to impact technology, a number of studies have focused on the fundamental properties of SWNTs, with a growing component of this effort being devoted to their spectroscopic and photophysical characteristics.^{23–35}

Figure 1 illustrates the electronic density of states (DOS) for a typical semiconducting nanotube. Although all semiconducting tubes have similar band diagrams, the energy spacing between bands is dictated by the tube chirality and diameter. Associated with each conduction band is an excitonic state (Ex₁₁, Ex₂₂, etc.) that corresponds to an electron–hole pair bound together through a mutual electrostatic interaction. In many inorganic

semiconductors, the exciton binding energy is relatively weak (tens of milli electronvolts); however, carrier confinement in SWNTs enhances electron–hole interactions and leads to excitons with large binding energies (400 meV) and small spatial extents (1–2 nm).^{32–35} Excitons play a central role in all of the SWNT optical properties, governing their absorption, emission, and scattering processes, and more than likely are responsible for the SWNTs large third-order nonlinear susceptibility, $\chi^{(3)}$.^{20–22} There are two types of excitons: (1) bound excitons that lie within the optical gap and (2) resonant excitons that are embedded in the continuum of the lower energy bands. Bound excitons are produced by low-energy excitation (cf. transition C in Figure 1) and are stable with respect to dissociation.³⁶ Resonant excitons are formed at higher excitation energies (cf. transitions A and B in Figure 1). They resonantly couple to the continuum states, rapidly dissociate into free carriers,^{33,34} and then reassociate into the lowest energy excitonic state.^{37–39}

The exciton dynamics that occur following photoexcitation have been studied on a range of time scales using a variety of ultrafast spectroscopic methods.^{37–68} Experiments performed with 10 fs excitation pulses show that resonant excitons relax into the Ex₁₁ state on an approximately 50 fs time scale.^{37–39} Transient spectroscopies on longer time scales have identified the presence of several distinct kinetic components, including a fast 100–200 fs component, a slower 1 ps component, and in a few studies on isolated SWNTs, a long (>100 ps) decay. Despite the growing number of papers devoted to the subject,

* Corresponding author. E-mail: John_Papanikolas@unc.edu.

[†] University of North Carolina at Chapel Hill.

[‡] NASA Langley Research Center.

a consistent interpretation of the transient data has remained elusive, and many conflicting accounts still exist. The difficulty with interpretation arises in many experiments because the SWNTs are probed using single-wavelength detection methods, making it difficult to assign the different kinetic components in a multiexponential decay to a specific physical process.

We used femtosecond transient absorption (TA) spectroscopy to probe the excited states of SWNT bundles embedded in polymer films.^{67,68} Our previous paper presented TA spectra over a limited region of the visible spectrum following excitation at 550 nm into the Ex₃₃ exciton. The current paper expands upon this work in several different ways: It extends the excitation wavelengths to include Ex₂₂ (900 nm) and Ex₁₁ (1800 nm) exciton generation and expands the range of probe wavelengths to include much of the visible and near-UV regions. The methodology used here differs from many previous studies in one major respect—we examined the evolution of the transient spectrum, not just single-wavelength kinetics. This enabled us to correlate the evolution of different spectroscopic features and to disentangle their contributions to the decay kinetics. Our analysis uncovered a fast 100–300 fs component that we assigned to plasmon relaxation in the metallic tubes, biphasic electron–hole recombination (i.e., exciton decay) with fast (1.5 ps) and slow (35 ps) time components, and a time-dependent spectral shift that may reflect exciton self-trapping.

One striking observation is from the carbon nanotube TA spectrum itself. The spectrum is highly structured, consisting of a series of narrow induced absorption (IA) and induced transmission (IT) peaks, and stands in stark contrast to the broad and nondescript bands exhibited by many complex heterogeneous systems. We first reported this spectrum two years ago,^{67,68} and since then, structured spectra have been observed by several other groups,^{59–62,65,66} yet a clear explanation of its origin has not been identified. In this paper, we present evidence that the structured spectrum arises from a nonlinear optical response that causes a photoinduced red-shift in the exciton transition frequency when a second electron–hole pair is excited in the presence of an already existing exciton.

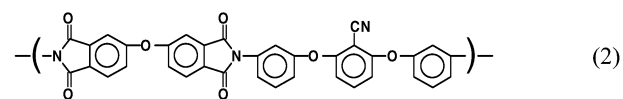
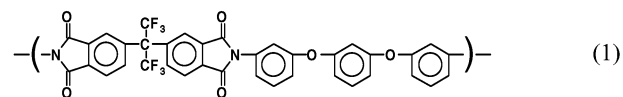
Work on inorganic systems has identified a variety of nonlinear mechanisms that can alter the optical properties of excitonic transitions,⁶⁹ including the formation of multiexcitonic species such as biexcitons⁷⁰ and four-particle excitations consisting of two electron–hole pairs (e,h;e,h) bound together by Coulombic and exchange interactions. In bulk semiconductors, these 2e–2h excitations are weakly bound, and detection of the biexcitonic state is difficult, even at low temperatures. This is not the case in nanostructures, where carrier confinement enhances the interaction between electrons and holes and leads to stronger binding energies. In fact, a variety of multiexcitonic species, including biexcitons, triexcitons, and even four-exciton complexes, are well-documented in quantum wells, wires, and dots formed from inorganic semiconductors.^{70–76} Often referred to as excitonic molecules, these excitations can exist in a range of electronic configurations that are akin to the ground and excited states found in molecular systems. The question thus arises: Do nanotubes support similar multiexcitonic states? Carrier confinement has led to speculation that such states do exist, with theoretical support coming from recent calculations,^{77,78} which suggest that like the exciton, the biexciton in nanotubes is strongly bound. The data described herein offer experimental corroboration for the presence of biexcitonic states in nanotubes.

Our data suggest that biexcitons are formed in the pump–probe experiment through a sequential two-photon excitation

process in which one photon is absorbed from the pump pulse and the other from the probe pulse. The result is a series of IA bands that correspond to the formation of biexcitons in different electronic states. The lowest energy transition, which lies outside our experimental detection window, produced biexcitons in their lowest energy configuration (i.e., the biexciton ground state). Induced absorption bands at higher probe photon energies, in the visible portion of the transient spectrum, are attributed to the formation of biexcitons with excited state configurations (e,h;e*,h*), analogous to those observed in inorganic systems.^{72–76} Our data suggest that nanotubes, like their inorganic counterparts, can support a manifold of multiexcitonic species.

Experimental Procedures

We studied nanotube bundles embedded in three different polymer matrices. The SWNTs were formed through laser ablation and have diameters of 0.8–1.1 nm. Generally speaking, carbon nanotubes form large bundles, and the bundles aggregate together to form ropes.¹ Our samples^{79,80} are comprised primarily of single bundles that are fairly small, on the order of 10–20 tubes, indicating that the polymers induce a significant degree of dispersion and debundling. The samples are all ~100 μm thick films of 0.1–0.5% (by wt) laser ablated SWNTs in either CP2, a colorless polyimide (**1**), β-CN APB/ODPA, a similar polymer with appended cyano groups (**2**), or poly(methyl methacrylate) (**3**).



The polymer–nanotube interactions in all three cases are limited to noncovalent forces. These interactions are weak in CP2 and PMMA but strong in β-CN APB/ODPA due to the presence of the CN functional groups.^{79,80} The transparent films used are optically clear and spatially homogeneous, when viewed by the naked eye. For comparison, we also examined SWNTs in the absence of the polymer environment by dissolving a 1% (by wt) SWNT-CP2 film in THF and dispersing the tubes in solution using an ultrasonic bath. For spectroscopic measurements, this suspension was circulated in a 2 mm cuvette with nitrogen gas to create a uniform sample during data acquisition. TA measurements performed on the THF suspensions yielded qualitatively identical spectra as the polymer composite films, indicating that local heating does not play a significant role. All measurements were performed at room temperature under ambient conditions.

The femtosecond TA instrument has been described in detail elsewhere.⁸¹ Briefly, the system is based on a Clark-MXR CPA-2001 Ti:sapphire 1 kHz regenerative amplifier that produces 150 fs laser pulses at 775 nm with pulse energies of approximately 900 μJ. The amplifier output was used as the input to an optical parametric amplifier (OPA) that is tunable between 1.0 and 2.0 μm. Excitation pulses at 900 nm were produced

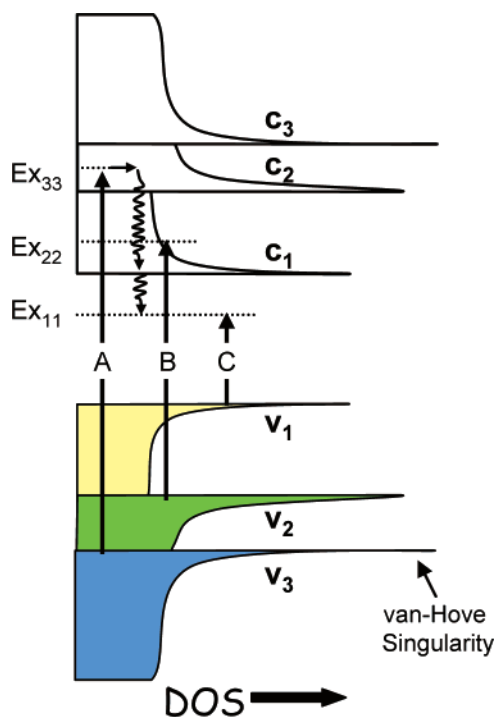


Figure 1. Illustration of the electronic DOS in semiconducting SWNTs. The sharp increases at the band edges, termed the van-Hove singularities, are a characteristic of one-dimensional systems. Arrows A–C represent optical transitions observed throughout the visible and near-infrared. Transitions A and B produce excitons that are resonantly coupled to the continuum of the lower energy bands and dissociate into free carriers; transition C forms a bound exciton.

via second-harmonic generation of the OPA output; 550 nm pulses were created by sum-frequency mixing of the OPA and regenerative amplifier beams. The pump beam was focused to an approximately 400–600 μm spot size at the sample. The probe pulse was a white-light supercontinuum generated in calcium fluoride that extended down to approximately 350 nm. The white light was split into two weaker beams that served as the signal and reference in the TA measurement. Both passed through the sample, but only the signal beam overlapped spatially with the pump beam. They were then dispersed by a 0.27 m monochromator and simultaneously detected by a two-dimensional liquid-nitrogen cooled CCD camera. This apparatus is capable of measuring a 70 nm portion of the transient spectrum between 350 and 1000 nm with a sensitivity of better than 1 mOD. The exciton dynamics were followed by obtaining TA spectra at a series of pump–probe delay times. Each spectrum was compensated to account for the frequency chirp in the white-light continuum, which was measured by detecting the optical Kerr response of liquid CCl_4 in a polarization gating geometry under identical conditions as the TA experiment. All experiments were conducted in a magic-angle pump–probe polarization configuration. Steady-state absorption spectra were collected using a Bio-Rad FTS6000 Fourier transform infrared spectrometer and a Shimadzu UV-1601 spectrometer.

Results and Discussion

This paper reports TA measurements of three different SWNT/polymer composites (CP2, β -CN APB/ODPA, and PMMA). The first section discusses the steady-state absorption spectroscopy. The excited state spectroscopy is presented in the second section, which details the origin of the structured

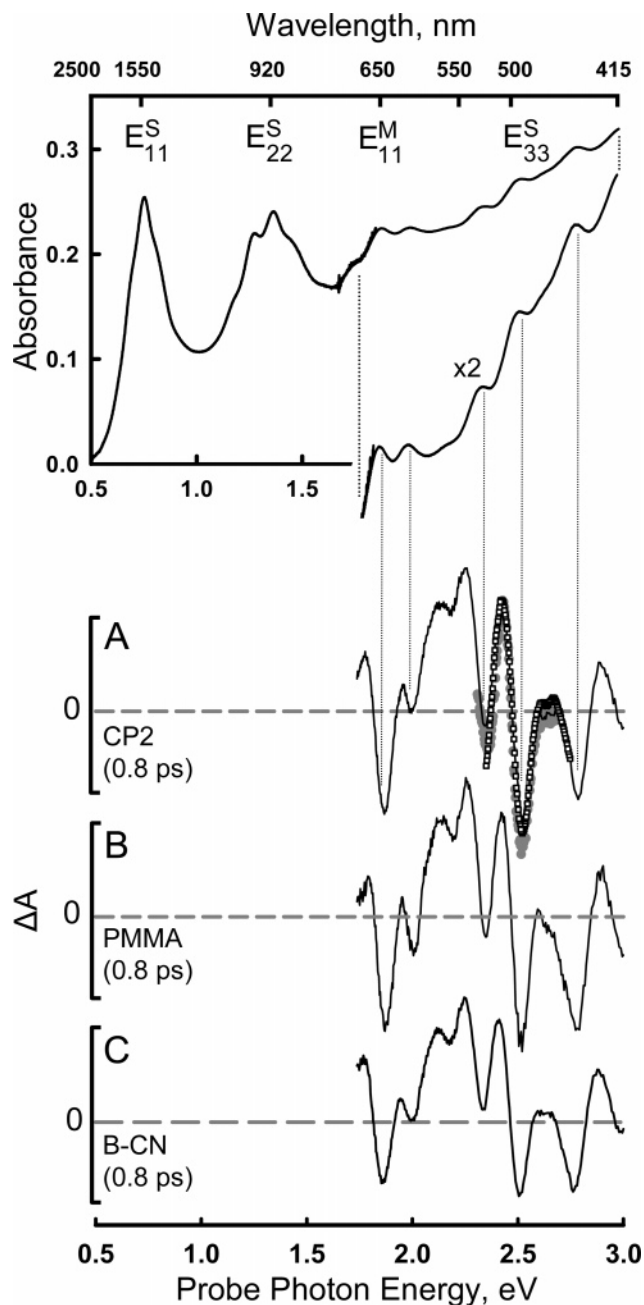


Figure 2. Ground state absorption spectrum of the SWNT/CP2 composite film (top panel). The bottom three panels (marked A–C) are the transient absorption spectra of the three different composites observed 0.8 ps after photoexcitation of the SWNTs; solid lines in all three panels correspond to excitation at 900 nm, and open squares and gray circles in part A correspond to excitation at 550 and 1800 nm, respectively.

spectrum and its evolution with time; it describes the dynamics of plasmon relaxation, exciton recombination, lattice reorganization, and the formation of biexcitons via a sequential two-photon absorption in the pump–probe experiment.

SWNT Ground State Spectroscopy. The ground state absorption spectrum of the SWNT/CP2 composite is shown in the top panel of Figure 2. The CP2 polymer is transparent for energies below 3 eV, and therefore, the carbon nanotubes are the only contributor to the absorption in this region of the spectrum. Furthermore, the absorption spectra obtained from the other polymer composites (not shown) are nearly identical, indicating that the nanotube electronic structure is not appreciably altered by incorporation into a matrix.

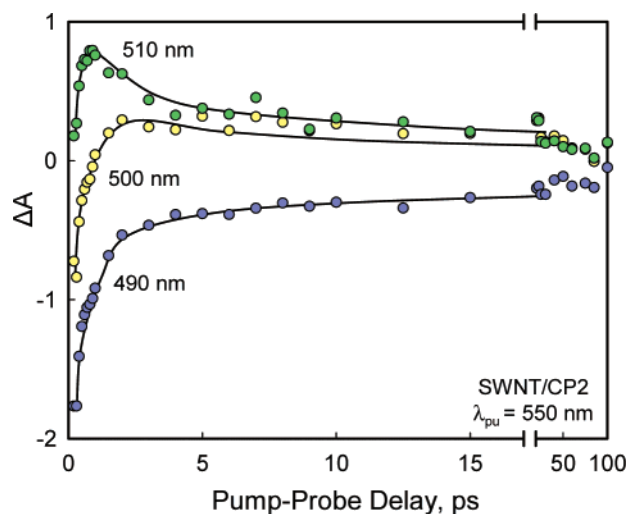


Figure 3. Transient absorption signal as a function of pump–probe delay for three different detection wavelengths. The transients exhibit complex kinetics, whose origin is described in the text.

The nanotube absorption spectrum consists of a series of broad bands (labeled E_{11}^S , E_{22}^S , E_{11}^M , and E_{33}^S) that appear on top of a wide background. The background is assigned to the red tail of a broad π -plasmon resonance that peaks at ~ 6 eV.⁸² This absorption corresponds to an optically driven coherent oscillation of electrons near the Fermi level and is analogous to the surface plasmon excitation observed in metallic nanoparticles.⁸³ The four absorption bands correspond to optical excitations in the nanotubes, and closer inspection reveals that each is a superposition of smaller features resulting from a distribution of nanotubes with varying diameters and chiral wrappings.

All SWNTs have increases in the DOS that result from the flattening of bands near the edges of the Brillouin zone (Figure 1) (i.e., the van-Hove singularities (vHs)).^{1,2} These structures establish band gaps in semiconducting tubes and pseudo-band gaps for metallic nanotubes. For some time, it was thought that the smaller features in the absorption spectrum arose from transitions between van-Hove singularities to produce spatially delocalized electronic states; however, it is now generally believed that optical excitation produces excitons with strong binding energies (400 meV) and small spatial extents (2 nm).^{32–35} Interestingly, the nature of the SWNT exciton is qualitatively different from excitons in bulk semiconductors where the binding energies are measured in tens of millielectronvolts.⁸⁴

Transient Absorption Spectroscopy. Pump–probe TA spectra obtained 800 fs after photoexcitation at 900 nm (E_{22}^S excitation) are displayed for each of the polymer environments in the lower three panels of Figure 2. Each spectrum is highly structured, showing a series of positive and negative features that correspond to IA and IT bands, respectively. TA spectra observed following excitation at 900 nm (E_{22}^S) and 550 nm (E_{33}^S) are nearly identical to the TA spectrum observed following 1800 nm (E_{11}^S) excitation (Figure 2a), suggesting the presence of rapid relaxation of the photoexcited charge carriers into a common final state, presumably the lowest energy exciton. This is consistent with the conclusions reached by other groups that placed the time scale for this relaxation process at approximately 50 fs.^{37–39} The IA and IT features in the TA spectrum thus correspond to transitions induced by the lowest energy exciton.

Spectral Evolution. Figure 3 shows the TA signal as a function of pump–probe delay for three different probe wavelengths. The curves exhibit complicated kinetics with both growth and decay components, consistent with the TA data reported by other groups.^{62,65} This complexity makes assignment of the kinetic components to physical phenomena, based solely on these single-wavelength transients, difficult. Our approach is to monitor the TA spectrum, which enables us to identify three distinct time-dependent features. The first is the decay of a broad IT band that occurs during the first 500 fs after excitation. This broad feature is discussed in greater depth in the *Supporting Information*. It is responsible for the upward trend in all three transients (Figure 3) at early times and is attributed to plasmon relaxation in the metallic nanotubes. The other features, which relate to the temporal evolution of the narrow IA and IT features, occur at longer times and are evident in the series of TA spectra displayed in the top panel of Figure 4. We observe both a decay of the IA and IT bands, as well as a time-dependent spectral shift associated with the IA bands. Although Figure 4a shows only a small portion of the TA spectrum, these features are repeated throughout the TA spectrum. We find that all of the IA and IT bands decay with the same kinetics regardless of probe wavelength, that the TA spectra and decay kinetics are independent of excitation intensity, and that each IA band exhibits a similar spectral shift. These three findings are discussed in more detail next.

IA/IT Decay Kinetics. Figure 4b shows the TA intensity at four different probe wavelengths as a function of pump–probe delay; the blue and green circles correspond to the IT and IA features in Figure 4a, while the yellow and red circles correspond to the decays of the IA and IT at 570 and 675 nm, respectively. Figure 4 shows the TA signal after 500 fs, when the contribution from the plasmon relaxation has subsided (see *Supporting Information*). After this time, the decays of the IA and IT features are the same regardless of probe wavelength, making the seemingly complex kinetics surprisingly simple. Our analysis, therefore, suggests that the differences at early time stem from the plasmon contribution to the TA signal rather than a complex interplay between multiple excitonic states.

The mirror image nature of the IA and IT decays signifies that both correspond to a single-dynamical process, presumably the destruction of the exciton, through electron–hole recombination. The decay is characterized by two decay times, a fast ~ 1.3 ps component as well as a slower 35 ps component. The fast component is consistent with observations of 1 ps relaxation rates by other laboratories, who, on the basis of single-wavelength measurements, assigned it to an assortment of different processes;^{45–48} the slow component is not typically observed in bundled SWNTs, although similar time scales (and longer) for recombination have been measured in studies where the nanotubes are encapsulated in micelles.⁵⁷ The presence of two time components suggests that there are two different relaxation pathways. Although the physical nature of these pathways is unknown, they may stem from enhanced relaxation via inter-tube phenomena (e.g., deactivation via metallic tubes) and/or exciton interaction with defect sites.

Intensity Dependence. Figure 5 shows TA spectra and decay kinetics obtained at two different excitation intensities. As described in the *Supporting Information*, intensity-dependent signals arising from plasmon excitation were observed during the first 500 fs. However, on longer time scales, neither the positions of the IA and IT bands in the TA spectra nor their decays depend upon the excitation intensity, suggesting that the structured spectrum does not depend upon exciton density and

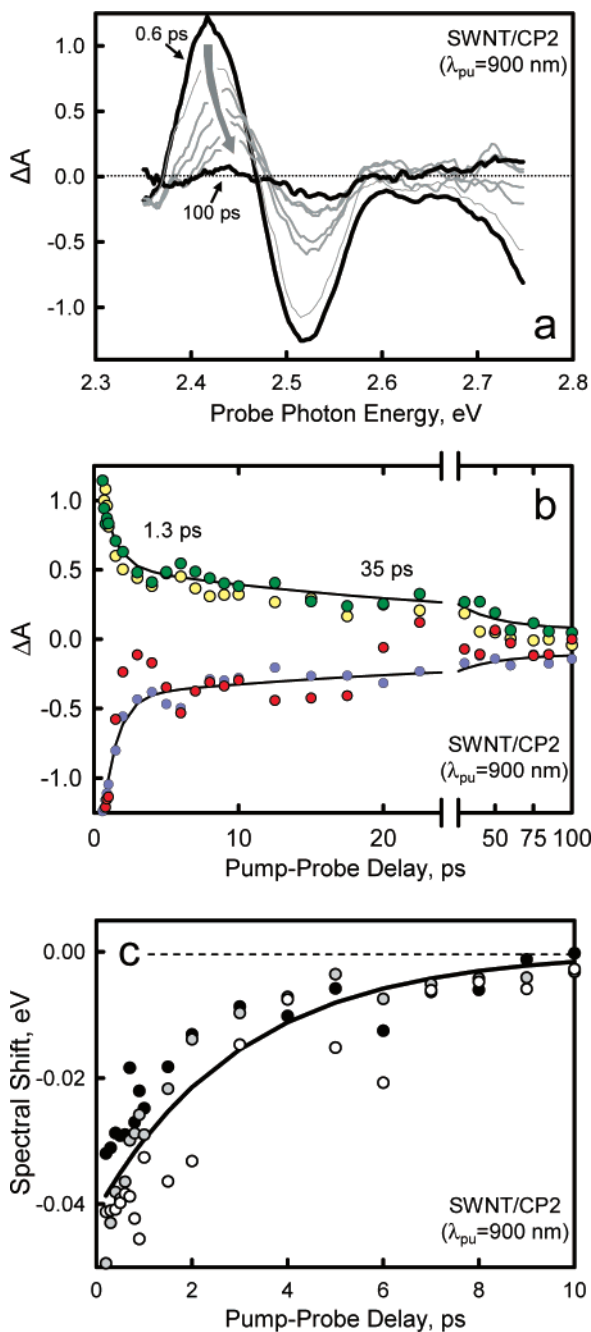


Figure 4. (a) Transient absorption spectra for the SWNT/CP2 composite obtained at different pump-probe delays between 0.6 and 100 ps. The spectra displayed represent a small portion of the total TA spectrum shown in Figure 2. The main observation in this time domain is the decay of the IA and IT features. Also apparent in the spectral evolution is a dynamical blue-shift of the IA feature by approximately 40 meV. (b) TA intensity for two IA and IT bands as a function of pump-probe delay. The detection wavelengths are 490 nm (blue), 510 nm (green), 570 nm (yellow), and 675 nm (red). Decays are biphasic with fast (1.3 ps) and slow (35 ps) components. (c) Time dependence of the spectral shift for three different IA bands; shown are 690 nm (open circles), 550 nm (gray circles), and 512 nm (solid circles). The shift is defined as $\hbar\omega(100 \text{ ps}) - \hbar\omega(t)$, where $\hbar\omega(t)$ is the IA band energy at time, t . The solid line is a fit to a single-exponential function with a 2.8 ps time constant. Although only three of the bands are shown, all of the IA features exhibit similar shifts, both in magnitude and in decay kinetics.

that the observed recombination dynamics arise from single-exciton processes. In contrast to our observations, several groups have reported intensity-dependent effects on the TA kinetics from individual, isolated SWNTs. Ma et al.^{57,60–62} reported a

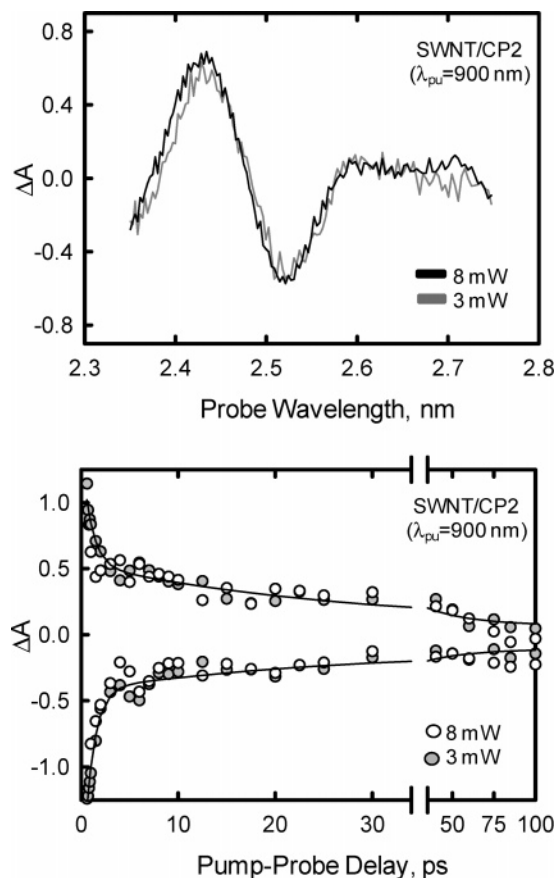


Figure 5. SWNT/CP2 transient absorption spectra (top) and decay kinetics (bottom) obtained at two different excitation intensities at 900 nm. The positive transients depict the amplitude of the IA band at a photon energy of 2.43 eV (510 nm), and negative transients correspond to the IT at 2.53 eV (490 nm).

nonlinear intensity dependence in the amplitude of the TA signal at early times and attributed it to exciton-exciton annihilation occurring on a sub-300 fs time scale. Krauss and Huang⁵¹ reported intensity-dependent kinetics between 2 and 10 ps that they ascribed to Auger recombination. It is unclear why we do not observe similar effects in our data; perhaps their absence stems from a greater effectiveness of SWNT bundles (rather than isolated tubes) to inhibit multiexciton deactivation processes.

IA Spectral Shift. Superimposed on top of the amplitude decay is a 35–40 meV shift of the IA band to the blue during the first few picoseconds after photoexcitation. All of the IA features exhibited similar behavior, both in magnitude and decay kinetics. Figure 4c shows the time dependence of the shift for three of these features. A single-exponential fit yields a 2.8 ps time constant. The time-dependent spectral shifts have not been observed in previous ultrafast studies by other groups, and while its origin is unknown, it may reflect the dynamical distortion of the carbon lattice that occurs in response to the formation of the photoexcited exciton (i.e., exciton self-trapping).

Spectral Assignment. Assignment of the TA spectrum must account for the simultaneous appearance of all the IT bands at early times and the origin of the IA bands. All of the IT features in the nanotube spectrum correlate with ground state absorptions (Figure 2) and are thus reminiscent of molecular systems where photoexcitation produces a hole in the ground state population that results in the instantaneous photobleaching of the entire ground state spectrum. However, despite the attractiveness of this picture, simultaneous photobleaching of all the ground state

transitions is in conflict with a band description of the nanotube's electronic structure.

This inconsistency can be illustrated with a simple example. In the band picture, excitation of the E_{22}^S transition would remove population from the ν_2 band, resulting in a bleach at the E_{22}^S transition frequency. Since the population in the other valence sub-bands (e.g., ν_1 and ν_3) would remain unchanged, the E_{11}^S and E_{33}^S transitions would be missing in the photobleaching spectrum at the instant of photoexcitation. Although these transitions would initially be absent, they could appear on longer time scales as the holes transferred between the manifold of sub-bands. While holes could relax from ν_2 to ν_1 , they could not transfer to ν_3 because it is energetically uphill. Thus, one might anticipate the emergence of a bleach at the E_{11}^S transition frequency but not at the E_{33}^S transition frequency. Of course, the situation would be different for initial excitation of the E_{11}^S or E_{33}^S transitions. On the whole, this picture predicts a complex evolution of the photobleaching spectrum that is not observed in our data. Indeed, our spectra indicate that regardless of the excitation wavelength, all of the IT bands, indeed the entire transient spectrum including photobleaches that lie to the blue of the excitation wavelength, appear within a time shorter than our instrument response (200 fs). This suggests that the IT bands are not simply a manifestation of a population hole introduced by photoexcitation.

Nonlinear Optical Response. The derivative-like nature suggests an alternative explanation: The TA spectrum arises from a nonlinear optical response in the carbon nanotubes. Generally speaking, such phenomena refer to a change in an optical transition (either its frequency or line width) in response to a resonant or nonresonant excitation. Studies on a variety of inorganic semiconductor materials show the existence of many possible nonlinear mechanisms.^{69–71}

The nature of the nonlinear response depends upon whether virtual or real populations are created.⁶⁹ A virtual population is only present during the excitation pulse, and thus, the persistence of the structured TA spectrum at long pump–probe delays rules out virtual states and eliminates mechanisms such as the optical Stark effect. Real populations (i.e., free carriers and/or excitons) persist for longer periods of time, and their existence can alter the optical transitions of subsequent excitations. This picture is similar in some respects to spectral changes observed in Stark spectroscopy, where the electronic transition is modified by an externally applied electric field,⁸⁵ yet is inherently more complicated as several processes could contribute, including Coulomb screening, phase-space filling, and carrier exchange interactions. These mechanisms arise from the interaction of an optical excitation with a collection of carriers (e.g., an electron–hole plasma). Another possibility is the production of biexcitonic and higher-order multiexcitonic species, which are akin to doubly excited states in molecular systems.^{69–71} Generally speaking, the spectroscopic signatures associated with nonlinear optical phenomena are either a shift in the transition frequency and/or an increase in its line width. The effect that these would have on the transient absorption spectrum is illustrated in Figure 6.

A photoinduced increase in the line width of the transition would lead to a symmetric TA spectrum with an IT band centered at the ground state transition frequency and weaker IA features to both higher and lower photon energies (Figure 6). The TA spectra shown in Figure 2 have this general shape, which at first glance would seem to implicate line broadening. However, the time-dependent spectral shifts exhibited by the IA features are inconsistent with this mechanism. If the optical

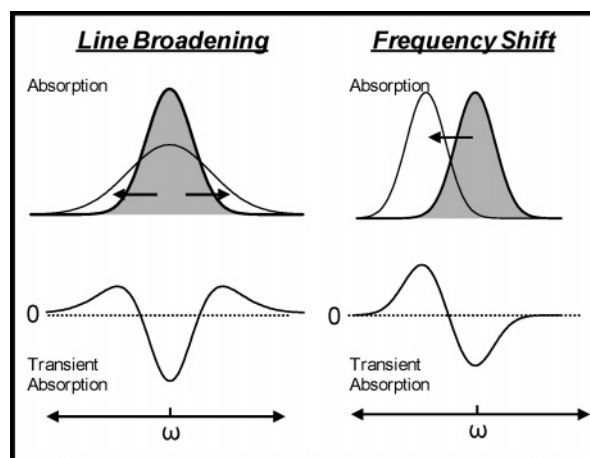


Figure 6. Illustration of the anticipated signatures in the TA spectrum resulting from a photoinduced increase in a transition's line width or a large shift in its transition frequency.

response derived from a line broadening mechanism, then this would imply that the time-dependent spectral shift observed in our TA data (Figure 4a) corresponds to a dynamic change in the line width of the transition. It follows then that a blue-shift of one feature should be mirrored by a red-shift in another. However, this is not observed in our TA spectra, where *all* of the IA bands exhibit blue-shifts of similar magnitude with increasing pump–probe delays (Figure 4c).

A photoinduced frequency shift, on the other hand, would result in asymmetric spectra containing both IA and IT features. When the shift exceeds the line width, the TA spectrum resembles the one shown in Figure 6 with an IT band at the ground state frequency and an IA band lying to the red or blue, depending upon the direction of the shift.⁸⁶

We explored the possibility of a photoinduced frequency shift by modeling the TA spectrum as the difference between shifted (ϵ_{sh}) and unshifted ground state spectra (ϵ_{gs}) (i.e., $\Delta A = (\epsilon_{sh} - \epsilon_{gs})$), representing the shifted spectrum simply by the ground state spectrum displaced along the energy axis by an amount δ . This is illustrated in the top panel of Figure 7. The calculated TA spectrum was then obtained by subtracting the unshifted spectrum (solid line in Figure 7) from the shifted one (dashed line in Figure 7). The result is shown for each of the polymers in the lower panels of Figure 7 along with its corresponding TA spectrum obtained at 0.8 ps. Given the simplicity of the model, the agreement is remarkable. Indeed, there is no reason a priori to assume a uniform red-shift in all of the transitions or that the shifted absorptions would have the same oscillator strength as their unshifted counterparts, yet this simple representation reproduces the oscillatory nature, line widths, and relative intensities observed in the data over a significant portion of the visible spectrum. The frequency shift model is also able to account for the spectral changes that occur with increasing pump–probe delay. Transient spectra at longer delays can be modeled by simply changing the magnitude of the red-shift (δ). For example, the TA spectrum of the CP2 composite at 1.8 ps can be reproduced using $\delta = .050$ eV (Figure 8).

Our analysis suggests that the IA and IT features ultimately are derived from a shift in the ground state absorptions. We thus propose the following interpretation of the TA spectrum: Excitons produced by photon absorption red-shift the transition frequencies of subsequent carrier excitations, resulting in a decrease in the absorption cross-section at the original transition frequencies (IT features) and a simultaneous increase at their new, red-shifted, locations (IA features). One question still remains: What is the physical origin of this optical nonlinearity?

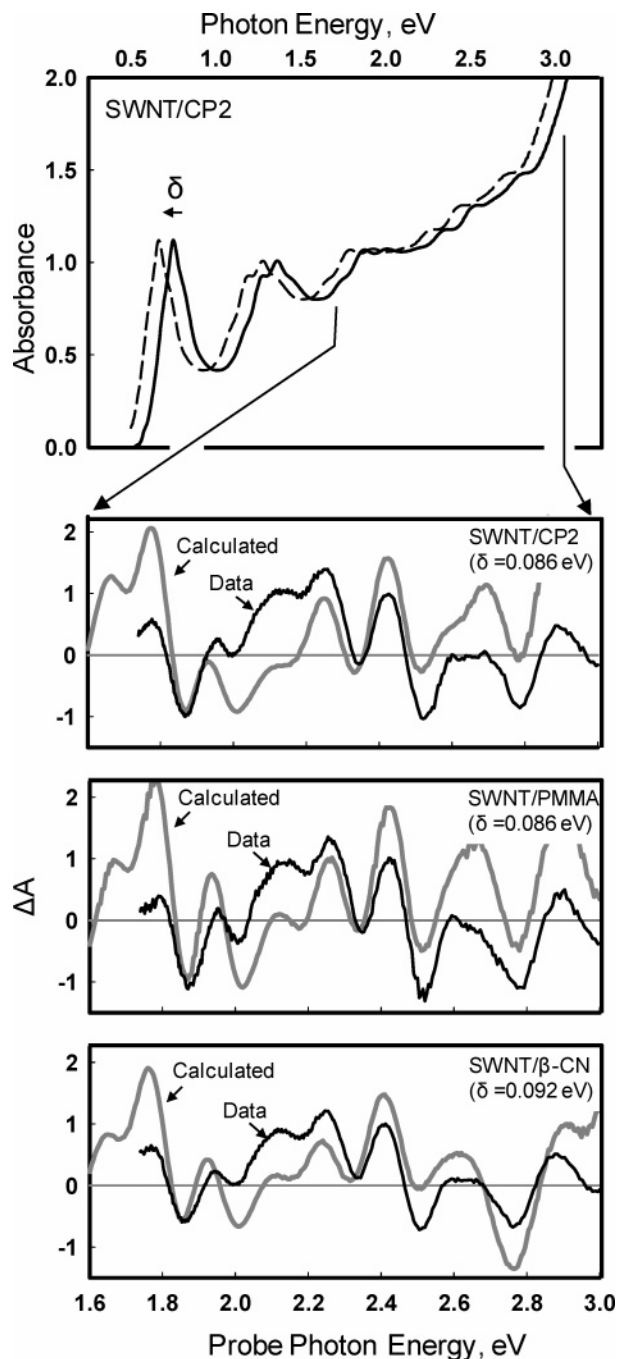


Figure 7. Illustration of the method used to simulate the transient absorption spectra by calculating the difference between shifted and unshifted ground state spectra. The top panel shows the ground state spectrum (solid line) and a copy of the shifted spectrum (dashed line). Displayed in the lower three panels are experimental TA data at 800 fs (black line) following the 900 nm excitation and calculated spectrum (gray line) for the three different polymers.

Biexciton Formation. Our observations are consistent with the formation of biexcitons, four-particle excitations consisting of two electrons and two holes bound together through Coulombic forces and exchange interactions. An energy diagram depicting the relationship between the excitonic and the biexcitonic states is shown in Figure 9. The single exciton and two noninteracting (spatially separated) excitons lie at energies E_x and $2E_x$ above the ground state, respectively. When the biexciton is stable with respect to dissociation into two free excitons, it lies at $2E_x - \epsilon_b$, where ϵ_b is the biexciton binding energy. In bulk semiconductors, this binding energy is small, and detection of the biexcitonic state is difficult, even at low temperatures.^{70,71}

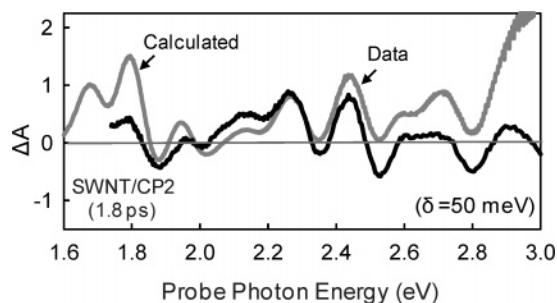


Figure 8. Experimental TA spectrum obtained 1.8 ps after 900 nm excitation of SWNT/CP2 (black line) and calculated spectrum (gray line) obtained with a 50 meV shift.

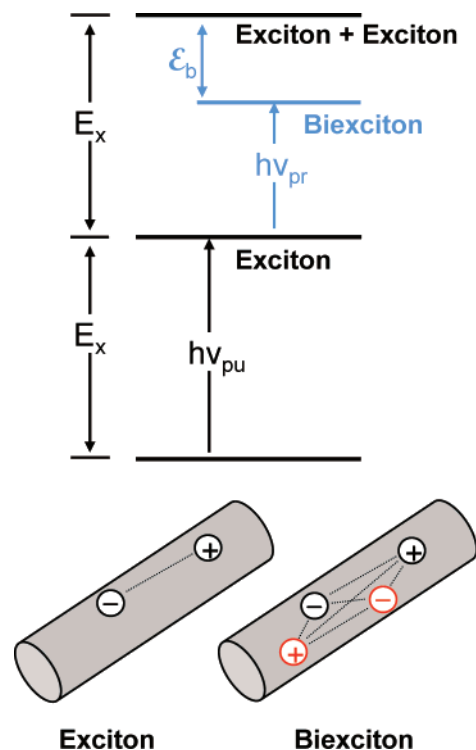


Figure 9. Energy diagram illustrating the ordering of the exciton and biexciton states. Excitons are a single electron–hole pair, whereas biexcitons are two electron–hole pairs bound together through electrostatic and exchange interactions. Biexcitons are stable with respect to dissociation into two free excitons by an amount, ϵ_b , the biexciton binding energy. In a pump–probe experiment, biexcitons can be formed through a sequential two-photon excitation by two different photon energies, $h\nu_{pu}$ and $h\nu_{pr}$.

However, carrier confinement in nanostructures (e.g., quantum wells and quantum dots) enhances the interaction between electrons and holes and leads to stronger binding energies than in bulk systems.^{70,71} Confinement effects are also at play in SWNTs, where biexcitons are predicted to be stable by 30–50 meV.^{77,78} It is this large stability that is ultimately responsible for the structured TA spectrum observed in the pump–probe experiment.

Generally speaking, biexcitons can be created via three different mechanisms.⁷⁰ Perhaps the most obvious is the condensation of two excitons accompanied by the emission of acoustic phonons. Although this process has been implicated in the excited states of SWNTs,⁶² it must compete with exciton–exciton annihilation and for this reason may not play a significant role. Biexcitons can also be formed via photoexcitation, either through (1) a single-step transition involving the simultaneous absorption of two photons at $1/2(2E_x - \epsilon_b)$ or (2) a two-step sequential process in which an exciton is first

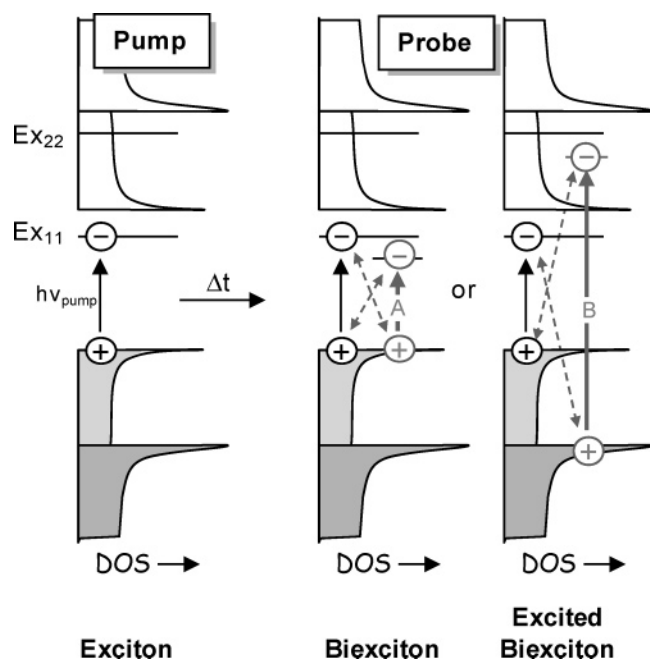


Figure 10. Illustration of biexciton formation in the SWNT pump-probe experiment. Excitation by the pump pulse produces an exciton, Ex_{11} . Subsequent excitation of an electron-hole pair in the same spatial region as the first exciton produces a biexciton, a four-particle excitation. The biexciton in SWNT is stabilized as compared to two free excitons, and thus, the optical transitions for the second absorption event are red-shifted relative to the first exciton transition. Our data suggest that biexciton transitions accompany all of the exciton bands. Two such transitions are indicated by the arrows A and B, which illustrate the formation of ground and excited state biexcitons, respectively.

created by absorption of a photon at E_x and then the absorption of a second, lower energy photon at $E_x - \epsilon_b$. It is the latter sequential excitation process that is responsible for the IA/IT features observed in the pump-probe TA spectrum (Figure 9). Although it appears in the state diagram (Figure 9) that the second photon is absorbed by the first exciton, it is important to realize that this is not the case: Biexciton formation in the pump-probe experiment is a sequential excitation that produces two electron-hole pairs in the same spatial location by two different photon absorption events.

The TA spectra observed here are consistent with biexciton formation in several key respects. First, the magnitude of the spectral shift observed in our TA spectra (50–90 meV), which is a direct measure of ϵ_b , is remarkably similar to the 30–50 meV binding energy predicted by Pedersen and co-workers.^{77,78} In fact, they predicted that the biexciton binding energy would exceed the line width of excitonic transition and that the resulting TA spectrum would resemble the one depicted in the right-hand side of Figure 6. Second, the magnitude of the shift is independent of the excitation intensity. For many nonlinear mechanisms that are derived from interactions with an electron-hole plasma, the magnitude of the spectral shifts scale with the charge carrier density, and hence, the excitation intensity. This is not the case for biexciton formation, where the size of the shift is determined by the biexciton binding energy. Under these circumstances, the TA spectrum should be independent of the excitation intensity, which is in fact what we observed.

Our data appear to take the concept of biexciton formation one step further. The Pedersen discussion^{77,78} focuses on the lowest energy transition (A in Figure 10), which produces the ground state biexciton. For the laser-ablated nanotubes used here, this IA band would appear at 1.6–1.7 μm , which lies outside our detection window. However, our analysis indicates that red-

shifted bands accompany all of the exciton transitions, not just the lowest energy one. These higher energy bands are attributed to the formation of biexcitons with excited state configurations ($e,h;e^*,h^*$) (cf. B in Figure 10). The presence of such species in nanotubes may not be that surprising given that the biexciton excited states have been detected in the absorption and emission spectra of several quantum confined systems.^{72–76} Pump-probe experiments on CuCl quantum dots, for example, identified IA bands lying to the red side of the higher-energy exciton bands⁷⁵ that were attributed to excited state biexcitons, and similar IA bands were observed in the TA spectra of CdS quantum dots.⁷⁴ In both cases, the transitions were similar to the ones observed in the nanotube samples. Taken together, our results suggest, for the first time, that nanotubes support a manifold of biexcitonic states and, at the same time, point to the potential existence of a host of multiexcitonic states, just as has been observed in a number of quantum confined systems.

The quantity δ is a measure of the biexciton binding energy, ϵ_b . Interestingly, its magnitude depends upon the polymer environment, exhibiting the largest shift in the β -CN APB/ODPA polymer ($\delta = 0.092$ eV) as compared to CP2 or PMMA ($\delta = 0.086$ eV). An even smaller shift ($\delta = 0.080$ eV) is observed when the CP2 film is dissolved in tetrahydrofuran (THF), which alters the nanotube environment by displacing CP2 with THF. Although the differences are small, they have been reproduced in multiple samples. The observation of spectral shifts that depend upon the host matrix suggests that interaction with the environment plays a role in the biexciton stability.

Red-shifted absorption features have not been discussed per se in the nanotube literature; however, they are not unique to our samples. Inspection of the transient data obtained in other laboratories,^{20,62–64} on both bundled and unbundled nanotubes, shows similar IA features on the low-energy side of the ground state absorption bands. It is important to recognize, however, that not all nanotube samples show these IA bands. For example, low-energy absorption bands are absent in recent TA experiments on isolated (6,5) nanotubes wrapped in DNA.⁸⁷ The reason for their absence in this system is unclear but could be an indication that biexcitonic states are not present in all nanotube types or that the DNA environment surrounding the tube weakens the biexciton to the point that it is no longer stable. Regardless, the appearance of red-shifted IA bands in other systems suggests that the presence of biexcitonic states in nanotubes is a fairly general phenomenon.

On the whole, our results suggest, for the first time, that nanotubes support a manifold of biexcitonic states with ground and excited state configurations. At the same time, it signifies the potential existence for a host of multiexcitonic states, just as has been observed in vast number of quantum confined systems.

Conclusion

We used femtosecond TA spectroscopy to examine the excited state dynamics of SWNT bundles embedded in polymer matrices. We observed a structured TA spectrum consisting of a series of narrow IT and IA bands. Analysis of the TA spectra suggests that it arises from a nonlinear optical response of the SWNT that we attribute to the sequential two-photon excitation of biexcitons (four-particle excitation involving two electrons and two holes) and excited biexcitons in the carbon nanotubes. From this perspective, the excitons produced by the pump pulse act as perturbation centers, modifying the transition frequencies of all the other carrier excitations in their local vicinity.

The exciton dynamics were followed by monitoring the TA spectra at a series of pump-probe delay times. We observed

three distinct spectral signatures in the time-dependent data: (1) the decay of a broad photobleach (assigned to plasmon relaxation); (2) the biphasic decay of the narrow IT and IA features (assigned to electron–hole recombination); and (3) a dynamical spectral shift of IA bands (attributed to lattice relaxation associated with exciton self-trapping).

Acknowledgment. Funding for this project was provided by the National Science Foundation (CHE-0301266) and the NASA University Research, Engineering and Technology Institute on Bio Inspired Materials (NCC-1-02037).

Supporting Information Available: Transient absorption spectrum for a series of pump–probe delays. This information is available free of charge via the Internet at <http://pubs.acs.org>.

References and Notes

- Dresselhaus, M. S.; Dresselhaus, G.; Avouris, P. *Carbon Nanotubes: Synthesis, Structure, Properties, and Applications*; Springer: Berlin, 2001.
- Saito, R.; Dresselhaus, G.; Dresselhaus, M. S. *Physical Properties of Carbon Nanotubes*; Imperial College Press: London, 1998.
- Baughman, R. H.; Zakhidov, A. A.; De Heer, W. A. *Science (Washington, DC, U.S.)* **2002**, *297*, 787.
- Collins, P. G.; Zettl, A.; Bando, H.; Thess, A.; Smalley, R. E. *Science (Washington, DC, U.S.)* **1997**, *278*, 100.
- Appenzeller, J.; Martel, R.; Derycke, V.; Radosavjevic, M.; Wind, S.; Neumayer, D.; Avouris, P. *Microelectron. Eng.* **2002**, *64*, 391.
- Bhattacharyya, S.; Kymakis, E.; Amaratunga, G. A. J. *Chem. Mater.* **2004**, *16*, 4819.
- Derycke, V.; Martel, R.; Appenzeller, J.; Avouris, P. *Nano Lett.* **2001**, *1*, 453.
- Kymakis, E.; Amaratunga, G. A. J. *Rev. Adv. Mater. Sci.* **2005**, *10*, 300.
- Kymakis, E.; Amaratunga, G. A. J. *J. Appl. Phys.* **2006**, *99*, 84302.
- Minoux, E.; Groening, O.; Teo, K. B. K.; Dalal, S. H.; Gangloff, L.; Schnell, J. P.; Hudanski, L.; Bu, I. Y. Y.; Vincent, P.; Legagneux, P.; Amaratunga, G. A. J.; Milne, W. I. *Nano Lett.* **2005**, *5*, 2135.
- Nakazawa, M.; Nakahara, S.; Hirooka, T.; Yoshida, M. *Opt. Lett.* **2006**, *31*, 915.
- Ouyang, M.; Huang, J. L.; Lieber, C. M. *Acc. Chem. Res.* **2002**, *35*, 1018.
- Patyk, R. L.; Lomba, B. S.; Nogueira, A. F.; Furtado, C. A.; Santos, A. P.; Mello, R. M. Q.; Micaroni, L.; Hummelgen, I. A. *Phys. Status Solidi RRL* **2007**, *1*, 43.
- Pradhan, B.; Batabyal, S. K.; Pal, A. J. *Appl. Phys. Lett.* **2006**, *88*, 93106.
- Rozhin, A. G.; Sakakibara, Y.; Namiki, S.; Tokumoto, M.; Kataura, H.; Achiba, Y. *Appl. Phys. Lett.* **2006**, *88*, 51118.
- Rueckes, T.; Kim, K.; Joselevich, E.; Tseng, G. Y.; Cheung, C. L.; Lieber, C. M. *Science (Washington, DC, U.S.)* **2000**, *289*, 94.
- Teo, K. B. K.; Lacerda, R. G.; Yang, M. H.; Teh, A. S.; Robinson, L. A. W.; Dalal, S. H.; Rupasinghe, N. L.; Chhowalla, M.; Lee, S. B.; Jefferson, D. A.; Hasko, D. G.; Amaratunga, G. A. J.; Milne, W. L.; Legagneux, P.; Gangloff, L.; Minoux, E.; Schnell, J. P.; Pribat, D. *IEEE Proc., Circuits Devices Syst.* **2004**, *151*, 443.
- Wind, S. J.; Appenzeller, J.; Avouris, P. *Phys. Rev. Lett.* **2003**, *91*, 58301.
- Wong, S. S.; Joselevich, E.; Woolley, A. T.; Cheung, C. L.; Lieber, C. M. *Nature (London, U.K.)* **1998**, *394*, 52.
- Maeda, A.; Matsumoto, S.; Kishida, H.; Takenobu, T.; Iwasa, Y.; Shimoda, H.; Zhou, O.; Shiraishi, M.; Okamoto, H. *J. Phys. Soc. Jpn.* **2006**, *75*, 43709.
- Maeda, A.; Matsumoto, S.; Kishida, H.; Takenobu, T.; Iwasa, Y.; Shiraishi, M.; Ata, M.; Okamoto, H. *Phys. Rev. Lett.* **2005**, *94*, 47404.
- Yi, W. H.; Feng, W.; Zhang, C. Y.; Long, Y. B.; Zhang, Z. G.; Li, B. M.; Wu, H. C. *J. Appl. Phys.* **2006**, *100*, 94301.
- Bachilo, S. M.; Strano, M. S.; Kittrell, C.; Hauge, R. H.; Smalley, R. E.; Weisman, R. B. *Science (Washington, DC, U.S.)* **2002**, *298*, 2361.
- Dresselhaus, M. S.; Dresselhaus, G.; Jorio, A.; Souza, A. G.; Pimenta, M. A.; Saito, R. *Acc. Chem. Res.* **2002**, *35*, 1070.
- Gruneis, A.; Saito, R.; Samsonidze, G. G.; Kimura, T.; Pimenta, M. A.; Jorio, A.; Souza, A. G.; Dresselhaus, G.; Dresselhaus, M. S. *Phys. Rev. B: Condens. Matter Mater. Phys.* **2003**, *67*, 165402.
- Jorio, A.; Pimenta, M. A.; Souza, A. G.; Saito, R.; Dresselhaus, G.; Dresselhaus, M. S. *New J. Phys.* **2003**, *5*, 139.
- Jorio, A.; Saito, R.; Hertel, T.; Weisman, R. B.; Dresselhaus, G.; Dresselhaus, M. S. *MRS Bull.* **2004**, *29*, 276.
- O'Connell, M. J.; Bachilo, S. M.; Huffman, C. B.; Moore, V. C.; Strano, M. S.; Haroz, E. H.; Rialon, K. L.; Boul, P. J.; Noon, W. H.; Kittrell, C.; Ma, J. P.; Hauge, R. H.; Weisman, R. B.; Smalley, R. E. *Science (Washington, DC, U.S.)* **2002**, *297*, 593.
- Rao, A. M.; Richter, E.; Bandow, S.; Chase, B.; Eklund, P. C.; Williams, K. A.; Fang, S.; Subbaswamy, K. R.; Menon, M.; Thess, A.; Smalley, R. E.; Dresselhaus, G.; Dresselhaus, M. S. *Science (Washington, DC, U.S.)* **1997**, *275*, 187.
- Sfeir, M. Y.; Beetz, T.; Wang, F.; Huang, L. M.; Huang, X. M. H.; Huang, M. Y.; Hone, J.; O'Brien, S.; Misewich, J. A.; Heinz, T. F.; Wu, L. J.; Zhu, Y. M.; Brus, L. E. *Science (Washington, DC, U.S.)* **2006**, *312*, 554.
- Sfeir, M. Y.; Wang, F.; Huang, L. M.; Chuang, C. C.; Hone, J.; O'Brien, S. P.; Heinz, T. F.; Brus, L. E. *Science (Washington, DC, U.S.)* **2004**, *306*, 1540.
- Perebeinos, V.; Tersoff, J.; Avouris, P. *Phys. Rev. Lett.* **2004**, *92*, 257402.
- Spataru, C. D.; Ismail-Beigi, S.; Benedict, L. X.; Louie, S. G. *Phys. Rev. Lett.* **2004**, *92*, 77402.
- Spataru, C. D.; Ismail-Beigi, S.; Benedict, L. X.; Louie, S. G. *Appl. Phys. A: Mater. Sci. Process.* **2004**, *78*, 1129.
- Wang, F.; Dukovic, G.; Brus, L. E.; Heinz, T. F. *Science (Washington, DC, U.S.)* **2005**, *308*, 838.
- Mohite, A.; Lin, J. T.; Sumanasekera, G.; Alphenaar, B. W. *Nano Lett.* **2006**, *6*, 1369.
- Manzoni, C.; Gambetta, A.; Menna, E.; Meneghetti, M.; Lanzani, G.; Cerullo, G. *Phys. Rev. Lett.* **2005**, *94*, 207401.
- Lanzani, G.; Cerullo, G.; Gambetta, A.; Manzoni, C.; Menna, E.; Meneghetti, M. *Synth. Met.* **2005**, *155*, 246.
- Seferyan, H. Y.; Nasr, M. B.; Senekerimyan, V.; Zadayan, R.; Collins, P.; Apkarian, V. A. *Nano Lett.* **2006**, *6*, 1757.
- Ostojic, G. N.; Zaric, S.; Kono, J.; Strano, M. S.; Moore, V. C.; Hauge, R. H.; Smalley, R. E. *Phys. Rev. Lett.* **2004**, *92*, 117402.
- Kono, J.; Ostojic, G. N.; Zaric, S.; Strano, M. S.; Moore, V. C.; Shaver, J.; Hauge, R. H.; Smalley, R. E. *Appl. Phys. A: Mater. Sci. Process.* **2004**, *78*, 1093.
- Huxtable, S. T.; Cahill, D. G.; Shenogin, S.; Xue, L. P.; Ozisik, R.; Barone, P.; Usrey, M.; Strano, M. S.; Siddons, G.; Shim, M.; Keblinski, P. *Nat. Mater.* **2003**, *2*, 731.
- Reich, S.; Dworzak, M.; Hoffmann, A.; Thomsen, C.; Strano, M. S. *Phys. Rev. B: Condens. Matter Mater. Phys.* **2005**, *71*, 033402.
- Hagen, A.; Moos, G.; Talalaev, V.; Hertel, T. *Appl. Phys. A: Mater. Sci. Process.* **2004**, *78*, 1137.
- Lauret, J. S.; Voisin, C.; Cassabois, G.; Delalande, C.; Roussignol, P.; Capes, L.; Jost, O. *Physica E (Amsterdam, Neth.)* **2003**, *17*, 380.
- Lauret, J. S.; Voisin, C.; Cassabois, G.; Delalande, C.; Roussignol, P.; Jost, O.; Capes, L. *Phys. Rev. Lett.* **2003**, *90*, 57404.
- Huang, L. B.; Pedrosa, H. N.; Krauss, T. D. *Phys. Rev. Lett.* **2004**, *93*, 17403.
- Korovyanko, O. J.; Sheng, C. X.; Vardeny, Z. V.; Dalton, A. B.; Baughman, R. H. *Phys. Rev. Lett.* **2004**, *92*, 17403.
- Hertel, T.; Fasel, R.; Moos, G. *Appl. Phys. A: Mater. Sci. Process.* **2002**, *75*, 449.
- Ichida, M.; Hamanaka, Y.; Kataura, H.; Achiba, Y.; Nakamura, A. *J. Phys. Soc. Jpn.* **2004**, *73*, 3479.
- Huang, L. B.; Krauss, T. D. *Phys. Rev. Lett.* **2006**, *96*, 57407.
- Gambetta, A.; Manzoni, C.; Menna, E.; Meneghetti, M.; Cerullo, G.; Lanzani, G.; Tretiak, S.; Piryatinski, A.; Saxena, A.; Martin, R. L.; Bishop, A. R. *Nat. Phys.* **2006**, *2*, 515.
- Sheng, C. X.; Vardeny, Z. V.; Dalton, A. B.; Baughman, R. H. *Synth. Met.* **2005**, *155*, 254.
- Sheng, C. X.; Vardeny, Z. V.; Dalton, A. B.; Baughman, R. H. *Phys. Rev. B: Condens. Matter Mater. Phys.* **2005**, *71*, 125427.
- Hagen, A.; Steiner, M.; Raschke, M. B.; Lienau, C.; Hertel, T.; Qian, H. H.; Meixner, A. J.; Hartschuh, A. *Phys. Rev. Lett.* **2005**, *95*, 197401.
- Ma, Y. Z.; Valkunas, L.; Bachilo, S. M.; Fleming, G. R. *Phys. Chem. Chem. Phys.* **2006**, *8*, 5689.
- Ma, Y. Z.; Stenger, J.; Zimmermann, J.; Bachilo, S. M.; Smalley, R. E.; Weisman, R. B.; Fleming, G. R. *J. Chem. Phys.* **2004**, *120*, 3368.
- Valkunas, L.; Ma, Y. Z.; Fleming, G. R. *Phys. Rev. B: Condens. Matter Mater. Phys.* **2006**, *73*, 115432.
- Ma, Y. Z.; Valkunas, L.; Dexheimer, S. L.; Bachilo, S. M.; Fleming, G. R. *Phys. Rev. Lett.* **2005**, *94*, 157402.
- Ma, Y. Z.; Valkunas, L.; Bachilo, S. M.; Fleming, G. R. *J. Phys. Chem. B* **2005**, *109*, 15671.
- Ma, Y. Z.; Spataru, C. D.; Valkunas, L.; Louie, S. G.; Fleming, G. R. *Phys. Rev. B: Condens. Matter Mater. Phys.* **2006**, *74*, 85402.
- Ma, Y. Z.; Valkunas, L.; Dexheimer, S. L.; Fleming, G. R. *Mol. Phys.* **2006**, *104*, 1179.
- Zhao, H.; Mazumdar, S.; Sheng, C. X.; Tong, M.; Vardeny, Z. V. *Phys. Rev. B: Condens. Matter Mater. Phys.* **2006**, *73*, 75403.

- (64) Chou, S. G.; DeCamp, M. F.; Jiang, J.; Samsonidze, G. G.; Barros, E. B.; Plantz, F.; Jorio, A.; Zheng, M.; Onoa, G. B.; Semke, E. D.; Tokmakoff, A.; Saito, R.; Dresselhaus, G.; Dresselhaus, M. S. *Phys. Rev. B: Condens. Matter Mater. Phys.* **2005**, *72*, 195415.
- (65) Ellingson, R. J.; Engtrakul, C.; Jones, M.; Samec, M.; Rumbles, G.; Nozik, A. J.; Heben, M. J. *Phys. Rev. B: Condens. Matter Mater. Phys.* **2005**, *71*, 115444.
- (66) Russo, R. M.; Mele, E. J.; Kane, C. L.; Rubtsov, I. V.; Therien, M. J.; Luzzi, D. E. *Phys. Rev. B: Condens. Matter Mater. Phys.* **2006**, *74*, 41405.
- (67) Styers-Barnett, D. J.; Ellison, S. P.; Park, C.; Wise, K. E.; Papanikolas, J. M. *J. Phys. Chem. A* **2005**, *109*, 289.
- (68) Styers-Barnett, D. J.; Ellison, S. P.; Park, C.; Wise, K. E.; Papanikolas, J. M. Ultrafast Transient Absorption Spectroscopy Investigations of Excited State Dynamics in SWNT/Polymer Composites. In *Functional Carbon Nanotubes*; Materials Research Society Symposia Proceedings: Boston, MA, 2005.
- (69) Schmitt-Rink, S.; Chemla, D. S.; Miller, D. A. B. *Adv. Phys.* **1989**, *38*, 89.
- (70) Yoffe, A. D. *Adv. Phys.* **2001**, *50*, 1.
- (71) Axt, V. M.; Kuhn, T. *Rep. Prog. Phys.* **2004**, *67*, 433.
- (72) Kulakovskii, V. D.; Bayer, M.; Michel, M.; Forchel, A.; Gutbrod, T.; Faller, F. *Usp. Fiz. Nauk* **1998**, *168*, 123.
- (73) Dekel, E.; Gershoni, D.; Ehrenfreund, E.; Spektor, D.; Garcia, J. M.; Petroff, P. M. *Phys. Rev. Lett.* **1998**, *80*, 4991.
- (74) Hu, Y. Z.; Koch, S. W.; Lindberg, M.; Peyghambarian, N.; Pollock, E. L.; Abraham, F. F. *Phys. Rev. Lett.* **1990**, *64*, 1805.
- (75) Ikezawa, M.; Matsumoto, Y.; Takagahara, T.; Nair, S. V. *Phys. Rev. Lett.* **1997**, *79*, 3522.
- (76) Labrie, D.; Karasyuk, V. A.; Nissen, M. K.; Pokrovskii, Y. E.; Thewalt, M. L. W. *Phys. Rev. B: Condens. Matter Mater. Phys.* **1993**, *47*, 1628.
- (77) Pedersen, T. G. *Fullerenes, Nanotubes, Carbon Nanostruct.* **2005**, *13*, 33.
- (78) Pedersen, T. G.; Pedersen, K.; Cornean, H. D.; Duclos, P. *Nano Lett.* **2005**, *5*, 291.
- (79) Park, C.; Crooks, R. E.; Siochi, E. J.; Harrison, J. S.; Evans, N.; Kenik, E. *Nanotechnology* **2003**, *14*, 11.
- (80) Wise, K. E.; Park, C.; Siochi, E. J.; Harrison, J. S. *Chem. Phys. Lett.* **2004**, *391*, 207.
- (81) Shaw, G. B.; Brown, C. L.; Papanikolas, J. M. *J. Phys. Chem. A* **2002**, *106*, 1483.
- (82) Bursill, L. A.; Stadelmann, P. A.; Peng, J. L.; Prawer, S. *Phys. Rev. B: Condens. Matter Mater. Phys.* **1994**, *49*, 2882.
- (83) Link, S.; El-Sayed, M. A. *J. Phys. Chem. B* **1999**, *103*, 8410.
- (84) Scholes, G. D.; Rumbles, G. *Nat. Mater.* **2006**, *5*, 683.
- (85) Bublitz, G. U.; Boxer, S. G. *Annu. Rev. Phys. Chem.* **1997**, *48*, 213.
- (86) Small shift yields a transient spectrum that is similar to the first-derivative of the ground state band, exhibiting a zero-crossing at its center frequency. This is not observed in our data, however.
- (87) Zhu, Z. P.; Crochet, J.; Arnold, M. S.; Hersam, M. C.; Ulbricht, H.; Resasco, D.; Hertel, T. *J. Phys. Chem. C* **2007**, *111*, 3831.